

## Article

# Nd<sup>3+</sup>, Yb<sup>3+</sup>:YF<sub>3</sub> Optical Temperature Nanosensors Operating in the Biological Windows

Maksim Pudovkin , Ekaterina Oleynikova, Airat Kiiamov , Mikhail Cherosov and Marat Gafurov 

Institute of Physics, Kazan Federal University, 18th Kremlyovskaya Street, Kazan 420008, Russia

\* Correspondence: jaz7778@list.ru (M.P.); mgafurov@gmail.com (M.G.)

**Abstract:** This work is devoted to the study of thermometric performances of Nd<sup>3+</sup> (0.1 or 0.5 mol.%), Yb<sup>3+</sup> (X%):YF<sub>3</sub> nanoparticles. Temperature sensitivity of spectral shape is related to the phonon-assisted nature of energy transfer (PAET) between Nd<sup>3+</sup> and Yb<sup>3+</sup>). However, in the case of single-doped Nd<sup>3+</sup> (0.1 or 0.5 mol.%):YF<sub>3</sub> nanoparticles, luminescence decay time (LDT) of <sup>4</sup>F<sub>3/2</sub> level of Nd<sup>3+</sup> in Nd<sup>3+</sup> (0.5 mol.%):YF<sub>3</sub> decreases with the temperature decrease. In turn, luminescence decay time in Nd<sup>3+</sup> (0.1 mol.%):YF<sub>3</sub> sample remains constant. It was proposed, that at 0.5 mol.% the cross-relaxation (CR) between Nd<sup>3+</sup> ions takes place in contradistinction from 0.1 mol.% Nd<sup>3+</sup> concentration. The decrease of LDT with temperature is explained by the decrease of distances between Nd<sup>3+</sup> with temperature that leads to the increase of cross-relaxation efficiency. It was suggested, that the presence of both CR and PAET processes in the studied system (Nd<sup>3+</sup> (0.5 mol.%), Yb<sup>3+</sup> (X%):YF<sub>3</sub>) nanoparticles provides higher temperature sensitivity compared to the systems having one process (Nd<sup>3+</sup> (0.1 mol.%), Yb<sup>3+</sup> (X%):YF<sub>3</sub>). The experimental results confirmed this suggestion. The maximum relative temperature sensitivity was 0.9%·K<sup>-1</sup> at 80 K.

**Keywords:** lifetime thermometry; Nd<sup>3+</sup>, Yb<sup>3+</sup>:YF<sub>3</sub>; optical temperature sensors



**Citation:** Pudovkin, M.; Oleynikova, E.; Kiiamov, A.; Cherosov, M.; Gafurov, M. Nd<sup>3+</sup>, Yb<sup>3+</sup>:YF<sub>3</sub> Optical Temperature Nanosensors Operating in the Biological Windows. *Materials* **2023**, *16*, 39. <https://doi.org/10.3390/ma16010039>

Academic Editor: Toma Stoica

Received: 29 October 2022

Revised: 6 December 2022

Accepted: 16 December 2022

Published: 21 December 2022



**Copyright:** © 2022 by the authors. Licensee MDPI, Basel, Switzerland. This article is an open access article distributed under the terms and conditions of the Creative Commons Attribution (CC BY) license (<https://creativecommons.org/licenses/by/4.0/>).

## 1. Introduction

In our time, technological needs in various fields have reached such a development that conventional contact temperature sensors can no longer perform accurate measurements with submicrometer spatial resolution [1–3]. Traditional methods of temperature measuring are thermocouples, thermistors, and infrared cameras. They are not able to provide high spatial resolutions (rough estimation  $\sim\lambda/2$ ) and/or the required contactlessness. So, the development of new non-contact temperature sensors is mandatory in modern science and industry. In this case, the luminescence temperature sensing and/or mapping satisfies the above-mentioned requirements. In this method, the temperature determination can be performed by analyzing a temperature-dependent luminescence signal (in the majority of cases, these parameters are luminescence intensity, lifetime, and band shape) of the nano- or micro-sized phosphors which are in contact with the studied object. In its turn, working in the UV, visible and/or NIR spectral ranges allows obtaining submicrometer spatial resolution. Luminescent thermometry is highly required in medicine and biology [4,5] for thermography, for the clinical diagnosis of cancerous tumors [6], as well as for measuring the temperature of integrated circuits and micro devices in order to check their stability and proper functioning [1,2]. In this work, phosphors based on fluoride host doped with rare-earth ions are used. This class of materials has a high chemical stability, mechanical strength, sufficiently high melting point, relatively low probability of non-radiative processes [7], high quantum yield of luminescence [8], and low toxicity [9]. It should also be noted, that the modern methods of synthesis allows obtaining fluoride phosphors with desirable morphology and structure [10]. YF<sub>3</sub> host was chosen because of the low energy of phonons (500 cm<sup>-1</sup>), and, consequently, the low probability of multi-phonon non-radiative relaxation. Nd<sup>3+</sup> and Yb<sup>3+</sup> doping ions were chosen because of the

possibility of complex temperature-dependent energy exchange probabilities between the ions, which can provide high temperature sensitivity. Also, the excitation and emission wavelengths are situated in the near IR range (tissue transparency window), which is very important for biomedical applications [11]. Down-conversion optical temperature sensors based on  $\text{Nd}^{3+}/\text{Yb}^{3+}$  ion pair were recently studied in works [12–14]. In these phosphors, the emission of  $\text{Yb}^{3+}$  is observed under the  $\text{Nd}^{3+}$  excitation revealing the energy transfer between  $\text{Nd}^{3+}$  and  $\text{Yb}^{3+}$ . The luminescence intensity ratio (*LIR*) between  $\text{Nd}^{3+}$  emission ( ${}^4\text{F}_{3/2}$ – ${}^4\text{I}_{9/2}$  transition at ~866 nm) and  $\text{Yb}^{3+}$  emission ( ${}^2\text{F}_{5/2}$ – ${}^2\text{F}_{7/2}$  transition at ~980 nm) can be taken as a temperature-dependent parameter. The main mechanism of temperature sensitivity is related to the phonon-assisted nature of energy transfer between  $\text{Nd}^{3+}$  and  $\text{Yb}^{3+}$ . In the literature, there are three main energy transfer processes between the above-mentioned ions that can be characterized by their probabilities:  $W_{\text{ET}}$ —probability of energy transfer from  $\text{Nd}^{3+}$  to  $\text{Yb}^{3+}$ ,  $W_{\text{BET}}$ —probability of back energy transfer from  $\text{Yb}^{3+}$  to  $\text{Nd}^{3+}$ ,  $W_{\text{DIFF}}$ —probability of energy diffusion between  $\text{Yb}^{3+}$  ions [15]. In the case of a low concentration of  $\text{Nd}^{3+}$  energy transfer from  $\text{Nd}^{3+}$  to  $\text{Nd}^{3+}$  is considered to be negligible. The probabilities of above-mentioned energy transfer processes are competitive and they are dependent on doping ion concentrations. In particular,  $W_{\text{BET}}$  decreases with the increase of  $\text{Yb}^{3+}$  concentration. This phenomenon paves the way toward the manipulation of temperature sensitivity via  $\text{Yb}^{3+}$  concentration. Indeed, it was experimentally demonstrated in the works [12,14,16]. However, it seems, that the  $\text{Nd}^{3+}/\text{Yb}^{3+}$  doped phosphors are studied for relatively high  $\text{Yb}^{3+}$  concentrations (>1 mol.%). Specifically, in our previous work it was shown, that the emission of the sample  $\text{Nd}^{3+}$  (0.5%),  $\text{Yb}^{3+}$  (0.5%): $\text{YF}_3$  is negligible under  $\text{Nd}^{3+}$  excitation (355 nm,  ${}^4\text{I}_{9/2}$ – ${}^4\text{D}_{3/2}$  absorption band of  $\text{Nd}^{3+}$ ) and this sample was not studied. On the other hand, it can be suggested, that the excitation conditions (mostly excitation wavelength) could affect the relative emission intensities of both  $\text{Nd}^{3+}$  and  $\text{Yb}^{3+}$  and the intense  $\text{Yb}^{3+}$  emission can be observed for the samples, containing 1.0 mol.% of  $\text{Yb}^{3+}$  and even less. Indeed, the  $\text{Nd}^{3+}/\text{Yb}^{3+}$ -based optical sensor with lower  $\text{Yb}^{3+}$  concentrations (<1.0 mol.%) can demonstrate higher  $S_r$  and  $S_a$ . One of the highest  $S_r$  values obtained for  $\text{Nd}^{3+}$  (0.5%),  $\text{Yb}^{3+}$  (8.0%): $\text{YF}_3$  (~0.6%/K at 144 K) [12],  $\text{Nd}^{3+}$  (0.5%),  $\text{Yb}^{3+}$  (5.0%): $\text{LiLaP}_4\text{O}_{12}$  (~0.3%/K at 300 K) [15]. The double-doped inorganic nano- or microparticles are capable of demonstrating higher performances compared to their single-doped counterparts in the relatively broad temperature range of 10–400 K. Specifically,  $\text{Pr}^{3+}$ ,  $\text{Yb}^{3+}$ : $\text{LaF}_3$  down-conversion nanoparticles demonstrate one of the highest sensitivities ( $S_r$  ~ 6.0%·K<sup>-1</sup> at 10 K) in the cryogenic temperature range [17]. The high temperature sensitivity is attributed to the convenient phonon-assisted energy transfer as well as quantum cutting phenomenon. In its turn,  $\text{Nd}^{3+}$ ,  $\text{Yb}^{3+}$ : $\text{YPO}_3$  and  $\text{Nd}^{3+}$ ,  $\text{Yb}^{3+}$ : $\text{LaPO}_3$  phosphors are capable of reaching 1.2 and 1.0%·K<sup>-1</sup>, respectively at 300 K [18]. Here, the high temperature sensitivity is explained by the fact, that the efficiency of  $\text{Yb}^{3+}$  back energy transfer to  $\text{Nd}^{3+}$  increases with the increase of temperature that leads to the faster change of spectral-kinetic characteristics with temperature. In the case of  $\text{Tm}^{3+}$ ,  $\text{Yb}^{3+}$ : $\text{LiYF}_4$  down-conversion phosphors, they demonstrate maximum temperature sensitivities around 1.2%·K<sup>-1</sup> at 300 K. The high performance is explained by phonon-assisted energy transfer from  ${}^3\text{H}_4$  ( $\text{Tm}^{3+}$ ) to  ${}^2\text{F}_{5/2}$  ( $\text{Yb}^{3+}$ ). Note, that  $\text{Tm}^{3+}$ ,  $\text{Yb}^{3+}$  system has one of the biggest energy gap between interacting  ${}^3\text{H}_4$  ( $\text{Tm}^{3+}$ ) and  ${}^2\text{F}_{5/2}$  ( $\text{Yb}^{3+}$ ) levels around 2000 cm<sup>-1</sup>.

The objective of this work was to study physical background of functioning of the  $\text{Nd}^{3+}$ ,  $\text{Yb}^{3+}$ : $\text{YF}_3$  luminescent temperature sensors having different concentrations of doping ions. The tasks of the work were to investigate of the spectral-kinetic characteristics of  $\text{Nd}^{3+}$  and to calculate of the main characteristics of temperature sensors. In particular, the temperature evolution of luminescence spectra will be studied. The luminescence intensity ratio (*LIR*) of  $\text{Nd}^{3+}$  and  $\text{Yb}^{3+}$  emissions at different temperatures will allow concluding about energy exchange processes between  $\text{Nd}^{3+}$  and  $\text{Yb}^{3+}$  ions. The temperature evolution of luminescence decay curves of single-doped  $\text{Nd}^{3+}$ : $\text{YF}_3$  and double-doped  $\text{Nd}^{3+}$ ,  $\text{Yb}^{3+}$ : $\text{YF}_3$  will also allow concluding about energy exchange processes between the ions as well as

concluding about the contribution of other temperature-dependent processes related, for example, to the thermal expansion of crystal lattice.

We guess that the main novelty of the work is that the work deals with physical background of temperature sensitivity of spectral-kinetic characteristics of the studied  $\text{Nd}^{3+}$ ,  $\text{Yb}^{3+}:\text{YF}_3$  phosphors. However, most recent articles do not take into consideration the thermal expansion phenomenon. In the present paper, we make a hypothesis of temperature sensitivity based on conventional knowledge about phonon-assisted nature of energy transfer between  $\text{Nd}^{3+}$  and  $\text{Yb}^{3+}$  as well as on thermal expansion by demonstrating the lattice parameters change with the temperature.

## 2. Materials and Methods

$\text{Nd}^{3+}$  (0.1 or 0.5 mol.%),  $\text{Yb}^{3+}$  (X%): $\text{YF}_3$  (X = 0.5 and 1.0, 2.0, and 3.0 mol.%) nanoparticles were synthesized via a co-precipitation method with subsequent hydrothermal treatment (180 °C for 30 h) and annealing in vacuum at 500 °C for 5 h. The hydrothermal treatment is used to exclude different ammonium salts and form a pure single-phase  $\text{YF}_3$  doped sample. The annealing procedure improves crystallinity. For  $\text{Nd}^{3+}$  (0.5%),  $\text{Yb}^{3+}$  (8.0%): $\text{YF}_3$  3.5045 g of  $\text{Y}(\text{NO}_3)_3 \cdot 6\text{H}_2\text{O}$ , 0.0219 g of  $\text{Nd}(\text{NO}_3)_3 \cdot 6\text{H}_2\text{O}$ , 0.3737 g of  $\text{Yb}(\text{NO}_3)_3 \cdot 6\text{H}_2\text{O}$ , were dissolved in 80 mL of distilled water. Then the solution pH was adjusted to 2 with nitric acid. Thereafter, a water solution of  $\text{NH}_4\text{F}$  (1.4815 g of  $\text{NH}_4\text{F}$  was dissolved in 10 mL of distilled water) was added dropwise to the mixture while stirring on a magnetic stirrer (400 rpm). In the next step, the solution was treated by hydrothermal synthesis at 180 °C for 30 h. The precipitate was purified with distilled water by centrifugation. The resulting nanoparticles were dried in air at room temperature in a dustproof box. Then the phosphors were annealed in a vacuum at 500 °C for 5 h. The doping ion concentrations are represented in molar percentage (mol.%).

Morphology and size of the samples were studied via transmission electron microscope Hitachi HT7700 Exalens. Sample preparation: 10 microliters of the suspension were placed on a formvar/carbon lacey 3 mm copper grid; drying was performed at room temperature. After drying, the grid was placed on a transmission electron microscope using a special holder for microanalysis. The analysis was held at an accelerating voltage of 100 kV in TEM mode. We built a particle size distribution histogram via commonly used “Image J” software. Since the shape of the particles is not perfectly regular, we calculated the area (square nanometers) of each particle via 2D TEM image taking into consideration the scale bar. Then we equaled the value of the area to  $\pi \cdot D^2 / 4$  (the area of a circle) and extracted the D values. The statistics are based on the analysis of 100 particles. This method is useful in order to estimate the average size of non-spherical particles. The size distribution histogram was plotted in OriginPro 9.0 software. The size distribution histogram was fitted by LogNormal peak function from OriginPro 9.0 database that is commonly used for particle size analysis.

The phase composition of the particles was studied by means of X-ray diffraction method (XRD) using Bruker D8 ADVANCE X-ray diffractometer (Cu  $K_\alpha$  radiation,  $\lambda = 0.154$  nm) having Anton-Paar TTK 450 cooling chamber. We used liquid nitrogen as a cooling agent. The lattice parameter values were calculated in MAUD software (Material Analysis Using Diffraction). The luminescence spectra were recorded via a CCD spectrometer (StellarNet) (0.5 nm spectral resolution). The optical excitation of was performed via IR LD ( $\lambda_{\text{ex}} = 790$  nm, to  ${}^4\text{I}_{9/2} - {}^4\text{F}_{5/2}$ ,  $\text{Nd}^{3+}$  absorption band). The radiation was modulated by rectangular pulses with a period  $T = 30$  ms and pulse duration  $\tau = 5$  ms. The experiments were performed in the 80–320 K temperature range via so-called “cold finger” method. The temperature control was carried out via thermostatic cooler “CRYO industries” having LakeShore Model 325 (Westerville, OH, USA) temperature controller. The luminescence decay time curves were recorded via BORDO 211A digital oscillograph (10 bit and 200 MHz bandwidth), MDR-3 monochromator, and photomultiplier PEM-62 (working spectral range ~600–1200 nm). The power density of excitation irradiation was measured with PULSAR-2 powermeter using StarLab software. All the calculations were carried out via Origin.Pro.9.0 software.

In the optical experiments, it is important to avoid the heating of the sample. For this aim, the optimized power density of the excitation irradiation should be chosen. Here, this choice was based on the fact that the shape of the  $\text{Nd}^{3+}$  peak (850–910 nm,  $^4\text{F}_{3/2}$ – $^4\text{I}_{9/2}$  transition) in fluoride hosts ( $\text{YF}_3$  [13],  $\text{LaF}_3$  [19],  $\text{NaYF}_4$  [20]) is temperature-dependent. Hence, before each experiment, we recorded the  $\text{Nd}^{3+}$  peak (~845–925 nm) for several values of the laser irradiation power density. The luminescence spectra recorded at different values of power density are represented in (Supplementary Information Figure S1). The chosen power density was  $\sim 1300 \text{ W/m}^2$ . It should be noted, that due to the use of pulse laser irradiation, the values of the power density are averaged.

### 3. Results and Discussion

#### 3.1. Characterization of $\text{Nd}^{3+}$ , $\text{Yb}^{3+}:\text{YF}_3$ Phosphors

A transmission electron microscopy (TEM) image of the  $\text{Nd}^{3+}$  (0.1%): $\text{YF}_3$  particles and a size distribution histogram are represented in Figure 1a,b, respectively.

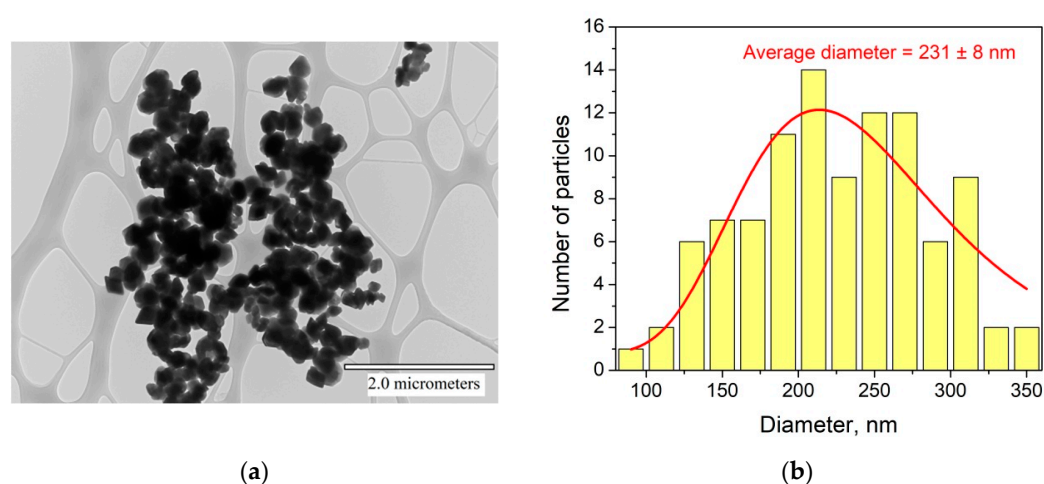


**Figure 1.** TEM image of  $\text{Nd}^{3+}:\text{YF}_3$  particles (a). Size distribution histogram of  $\text{Nd}^{3+}:\text{YF}_3$  particles (b) (fitting function is LogNormal from OriginPro.9.0. database).

According to the TEM image, the particles have relatively irregular shape reminding of the rhombus. The size distribution histogram is not perfectly fitted by any peak function, probably, due to the non-spherical shape of the particles. The LogNormal fitting determined  $231 \pm 8 \text{ nm}$  average diameter. The width of the size distribution histogram is around 130 nm. We also calculated the common average diameter of the particles (sum of sizes divided by the number of particles) that was equal to 201 nm. Anyway, the size of the particle is larger than 30 nm, hence, the influence of surface can be neglected [21]. Indeed, according to this work, the main unique difference between nanosized crystals and bulk ones is than the number of ions (here  $\text{Re}^{3+}$  and  $\text{F}^-$ ) located on the surface of the nanoparticles and the number of ions located in the nanoparticle volume are comparable. The rare-earth ions located on the nanoparticle's surface have different ligand surrounding compared to rare-earth ion inside the volume. The different surrounding leads to different spectral-kinetic properties. However, according to this work, for rare-earth trifluorides, for nanoparticles larger than 15 nm, the surface ions do not make a serious contribution in the spectral-kinetic properties in opposite to volume ions and nanoparticles are more similar to bulk crystals in term of spectral-kinetic properties. The phase composition of the  $\text{YF}_3$  doped particles was confirmed via XRD. In particular, XRD pattern of  $\text{Nd}^{3+}$  (0.1%): $\text{YF}_3$  sample detected for 100, 200, and 300 K and  $\text{YF}_3$  simulation are represented in Figure 2a,b, respectively. The XRD patterns agree with both the simulation and the reference pattern from the Inorganic Crystal Diffractions Database of orthorhombic  $\text{YF}_3$  ( $P_{nma}$  space group (no. 074–0911)).

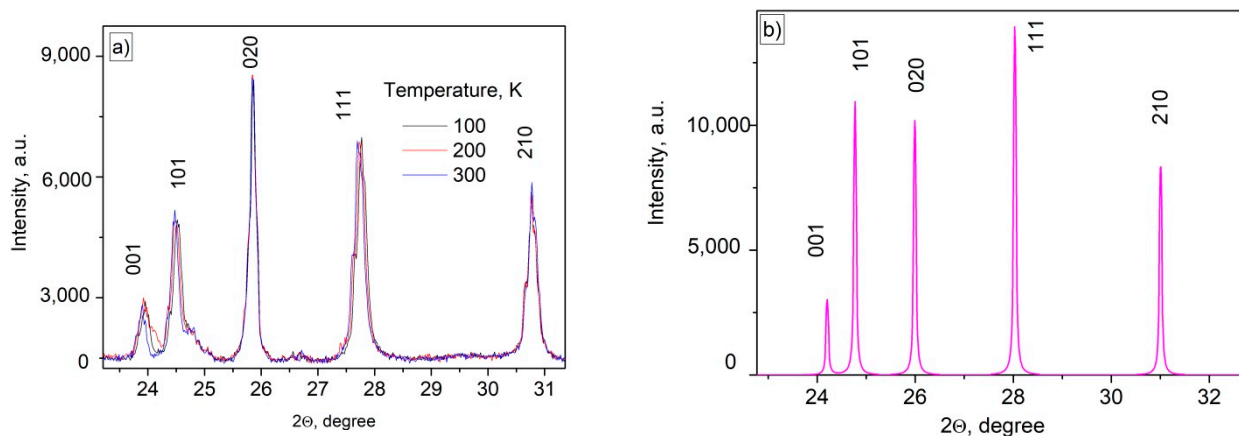


**Figure 2.** Experimental XRD patterns (a) of Nd<sup>3+</sup> (0.5%), Yb<sup>3+</sup> (1.0%):YF<sub>3</sub> sample and XRD simulation of YF<sub>3</sub> (b).

It can also be seen, that some XRD peaks shift toward higher angles with the temperature decrease that can be related to the lattice parameters decrease. Indeed, the calculated *a* constant values were 6.1300(2), 6.2109(3), and 6.3412(1) for 100, 200, and 300 K, respectively. The common shift of the nanoparticle XRD and the simulation of YF<sub>3</sub> XRD can be related to the presence of doping ions and captured water during the water-based synthesis procedure. It can be seen, that the lattice parameter change is in 0.1 nm/100K range. It can be suggested, that the distance between doping ions changes in the same range. Since, the nature of interaction between the doping ions is dipole-dipole, its efficiency is inversely proportional to *r*<sup>6</sup>, where *r* is the distance between interacting ions. It can be suggested, that such relatively small change in distances between the ions can affect the efficiency of interaction between them. For further development of this hypothesis we carried out spectral-kinetic characterization of both single-doped and double-doped samples.

An energy level diagram of the Nd<sup>3+</sup>/Yb<sup>3+</sup> ion pair is represented in Figure 3. The excitation wavelength λ<sub>ex</sub> = 790 nm corresponds to <sup>4</sup>I<sub>9/2</sub>–<sup>4</sup>F<sub>5/2</sub> absorption band of Nd<sup>3+</sup>.

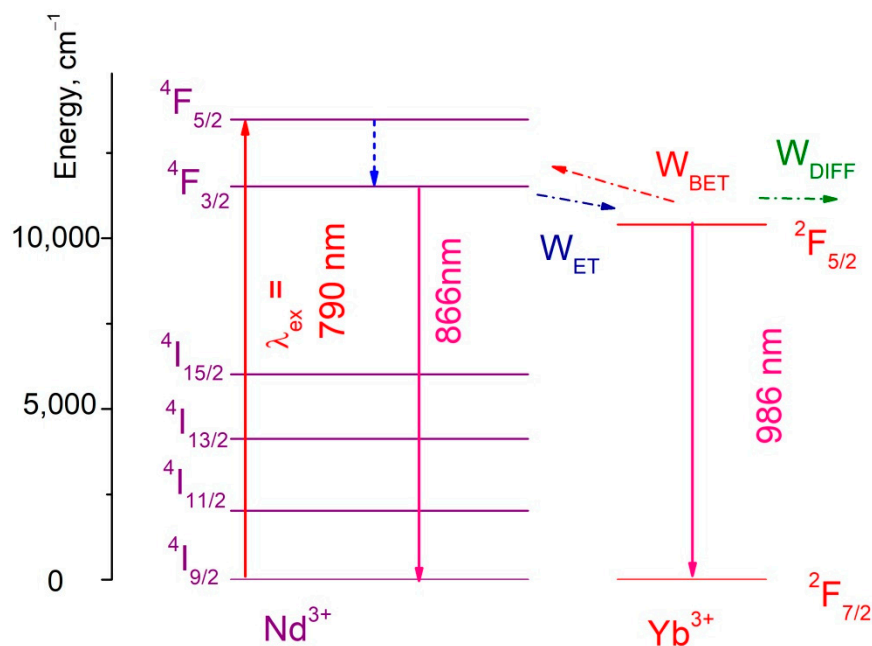


**Figure 3.** An energy level diagram of the Nd<sup>3+</sup>/Yb<sup>3+</sup> ion pair. Here W<sub>ET</sub>—probability of energy transfer from Nd<sup>3+</sup> to Yb<sup>3+</sup>, W<sub>BET</sub>—probability of back energy transfer from Yb<sup>3+</sup> to Nd<sup>3+</sup>, W<sub>DIFF</sub>—probability of energy diffusion between Yb<sup>3+</sup> ions.

As it was mentioned above, there are three main energy transfer processes between the doping ions that can be characterized by their probabilities:  $W_{ET}$ —probability of energy transfer from  $\text{Nd}^{3+}$  to  $\text{Yb}^{3+}$ ,  $W_{BET}$ —probability of back energy transfer from  $\text{Yb}^{3+}$  to  $\text{Nd}^{3+}$ ,  $W_{DIFF}$ —probability of energy diffusion between  $\text{Yb}^{3+}$  ions [15,18]. The energy transfer processes for  $\text{Nd}^{3+} \rightarrow \text{Yb}^{3+}$  and for  $\text{Yb}^{3+} \rightarrow \text{Nd}^{3+}$  are accompanied by emission or absorption of phonons, respectively. It provides the temperature sensitivity of the spectral-kinetic properties of the studied samples. In turn, the  $\text{Nd}^{3+}$  ions interact between each other via cross-relaxation mechanism ( ${}^4\text{F}_{3/2} - {}^4\text{I}_{15/2}$  and  ${}^4\text{I}_{9/2} - {}^4\text{I}_{15/2}$ ) that can also affect the temperature sensitivity.

### 3.2. Temperature Dependent Spectral-Kinetic Characterization of Single-Doped $\text{Nd}^{3+}:\text{YF}_3$ Nanoparticles and Microparticles

As we mentioned above, the cross-relaxation can also affect the temperature sensitivity. In order to exclude the cross-relaxation process, we synthesized a series of single-doped  $\text{Nd}^{3+}:\text{YF}_3$  samples having 0.1, 0.5, and 1.0 mol.% concentrations. As we mentioned above, the interplanar distances decrease with the decrease of temperature according to the XRD. Since, the cross-relaxation process is not phonon-assisted, it can be suggested, that the efficiency of cross-relaxation increases with the temperature decrease due to the fact that the distance between  $\text{Nd}^{3+}$  ions also decreases. The luminescence decay time curves detected at 100, 200, and 300 K for single-doped  $\text{Nd}^{3+}$  (0.1 (a), 0.5 (b), and 1.0 (c) mol.%): $\text{YF}_3$  nanoparticles are represented in Figure 4.

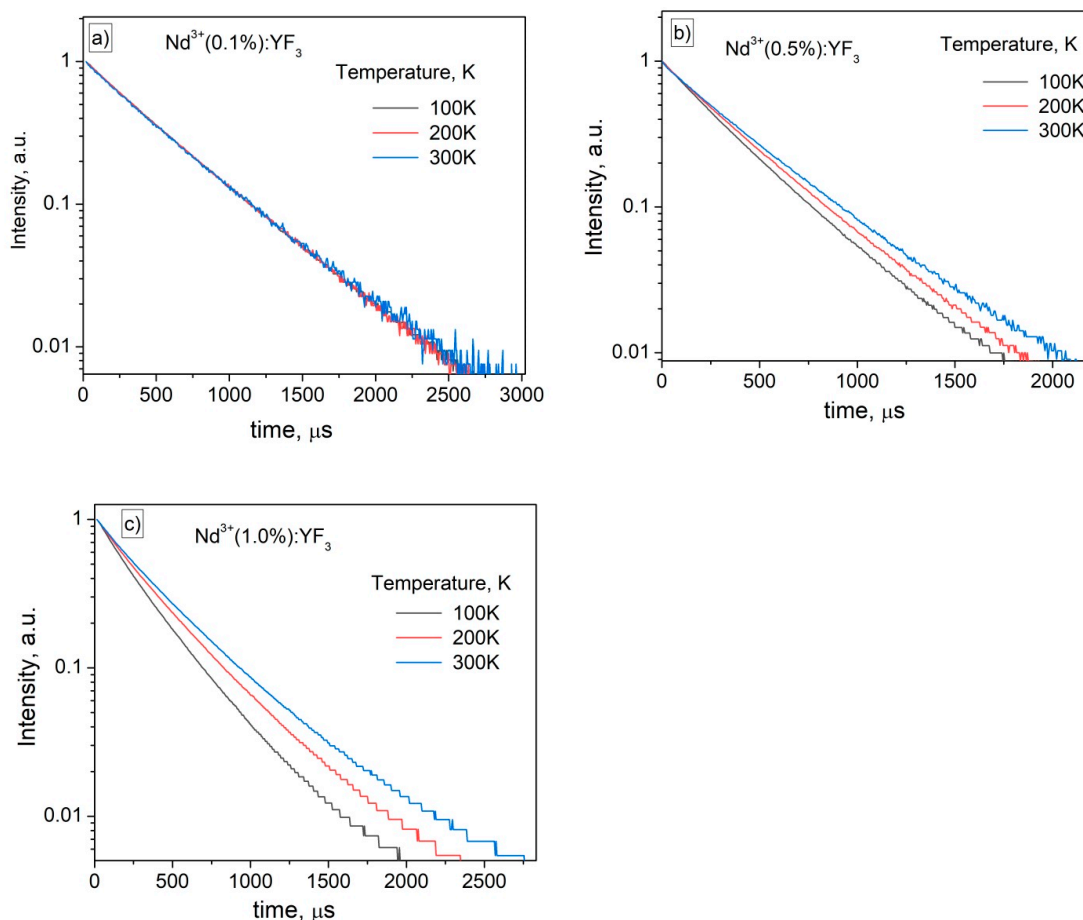


**Figure 4.** The luminescence decay time curves detected at 100, 200, and 300 K for single-doped  $\text{Nd}^{3+}$  (0.1 (a), 0.5 (b), and 1.0 (c) mol.%): $\text{YF}_3$  nanoparticles.  $\lambda_{ex} = 790 \text{ nm}$  ( ${}^4\text{I}_{9/2} - {}^4\text{F}_{5/2}$  absorption band of  $\text{Nd}^{3+}$ ),  $\lambda_{em} = 863 \text{ nm}$  ( ${}^4\text{F}_{3/2} - {}^4\text{I}_{9/2}$  emission band of  $\text{Nd}^{3+}$ ).

It can be seen, that for both  $\text{Nd}^{3+}$  (0.5 and 1.0 mol.%): $\text{YF}_3$  samples, decay time decreases with the temperature decrease. The curves can be well described by a single-exponential function. In particular, for  $\text{Nd}^{3+}$  (1.0 mol.%): $\text{YF}_3$  sample the decay times were 277, 328, and 358  $\mu\text{s}$  at 100, 200, and 300 K, respectively. In its turn, for  $\text{Nd}^{3+}$  (0.5 mol.%): $\text{YF}_3$  sample, the decay times were 370, 389, and 412  $\mu\text{s}$  at 100, 200, and 300 K, respectively. The  $\text{Nd}^{3+}$  (0.1 mol.%): $\text{YF}_3$  sample demonstrates  $\sim 472$   $\mu\text{s}$  decay time. The decrease of decay time with the increase of  $\text{Nd}^{3+}$  concentration can be explained by concentration quenching phenomenon.

It can be proposed, that at 0.5 mol.% the cross-relaxation between  $\text{Nd}^{3+}$  ions takes place in contradistinction from 0.1 mol.%  $\text{Nd}^{3+}$  concentration. The decrease of decay times with temperature can be explained by the decrease of distances between  $\text{Nd}^{3+}$  with temperature (thermal expansion phenomenon) that leads to the increase of cross-relaxation efficiency. It can be concluded, that for  $\text{Nd}^{3+}$  (0.1%): $\text{YF}_3$  nanoparticles the excitation energy does not scatter between  $\text{Nd}^{3+}$  ions. Since, the (1.0 mol.%): $\text{YF}_3$  showed the lowest signal-to-noise ratio, we chose 0.1 and 0.5%  $\text{Nd}^{3+}$  concentration in order to synthesize double doped  $\text{Nd}^{3+}$ ,  $\text{Yb}^{3+}$ : $\text{YF}_3$  and compare their performances.

### 3.3. Temperature Dependent Spectral-Kinetic Characterization of Double-Doped $\text{Nd}^{3+}$ , $\text{Yb}^{3+}$ : $\text{YF}_3$ Nanoparticles

To obtain high temperature sensor performances including relative ( $S_r$ ) temperature sensitivity, we synthesized a series of  $\text{Nd}^{3+}$  (0.1 mol.%),  $\text{Yb}^{3+}$  (0.5, 1.0, 2.0, and 3.0 mol.%): $\text{YF}_3$  samples. The choice of  $\text{Nd}^{3+}$  concentration is based on above-mentioned conclusions, that the excitation energy is not scattered between  $\text{Nd}^{3+}$  ions at 0.1 mol.% concentration. In turn, in order to provide comparable intensities of both  $\text{Nd}^{3+}$  and  $\text{Yb}^{3+}$  emissions the  $\text{Yb}^{3+}$  concentration was varied in the 0.5–3.0 mol.% range. At higher  $\text{Yb}^{3+}$  concentrations, its emission intensity was much higher than  $\text{Nd}^{3+}$  emission that led to deterioration of the performances. Indeed,  $\text{Nd}^{3+}$  (0.1 mol.%),  $\text{Yb}^{3+}$  (4.0 mol.%): $\text{YF}_3$  sample demonstrates almost negligible  $\text{Nd}^{3+}$  emission compared to  $\text{Yb}^{3+}$  one (Figure S2 of the Supplementary File). Normalized at 903 nm ( $\text{Nd}^{3+}$  emission peak) spectra of  $\text{Nd}^{3+}$  (0.1 mol.%),  $\text{Yb}^{3+}$  (1.0 mol.%): $\text{YF}_3$  sample recorded in the 80–320 K temperature range are represented in Figure 5.

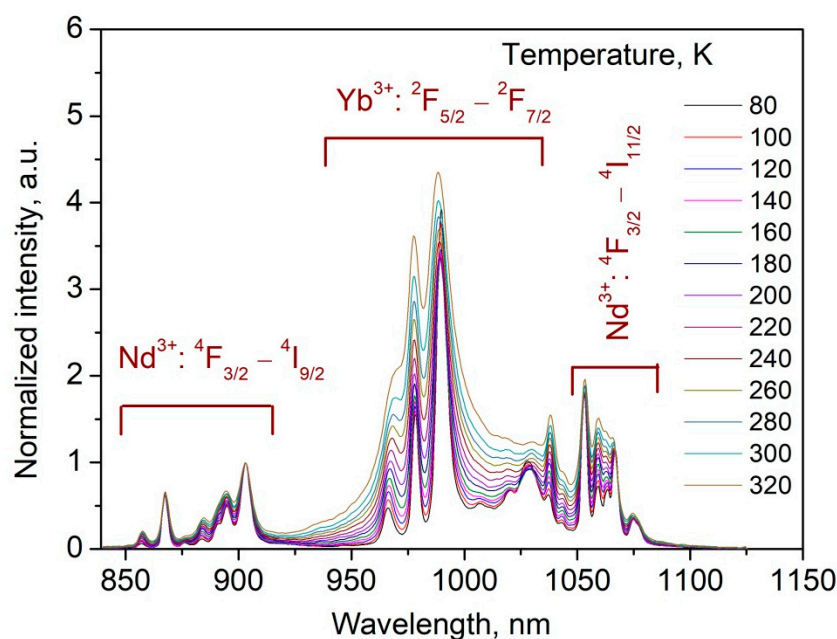


**Figure 5.** Normalized at 903 nm ( $\text{Nd}^{3+}$  emission peak) spectra of  $\text{Nd}^{3+}$  (0.1 mol.%),  $\text{Yb}^{3+}$  (1.0 mol.%): $\text{YF}_3$  sample recorded in the 80–320 K temperature range. 790 nm excitation wavelength corresponds to  $^4\text{I}_{9/2}$ – $^4\text{F}_{5/2}$  absorption band of  $\text{Nd}^{3+}$  ions.

It can be seen, that the spectral shape is notably dependent on temperature. In particular, the  $\text{Yb}^{3+}$  intensity increases with temperature increase compared to  $\text{Nd}^{3+}$  emission. It can be explained by the fact that the efficiency of phonon-assisted energy transfer from  $\text{Nd}^{3+}$  ( $^4\text{F}_{3/2}$ ) to  $\text{Yb}^{3+}$  ( $^2\text{F}_{5/2}$ ) increases with the temperature increase. Luminescence intensity ratio (*LIR*) between  $^4\text{F}_{3/2}$ – $^4\text{I}_{9/2}$  ( $\text{Nd}^{3+}$ ) and  $^2\text{F}_{5/2}$ – $^2\text{F}_{7/2}$  ( $\text{Yb}^{3+}$ ) was taken as a temperature-dependent parameter. The *LIR* curves as functions of temperature are represented in Figure 6.

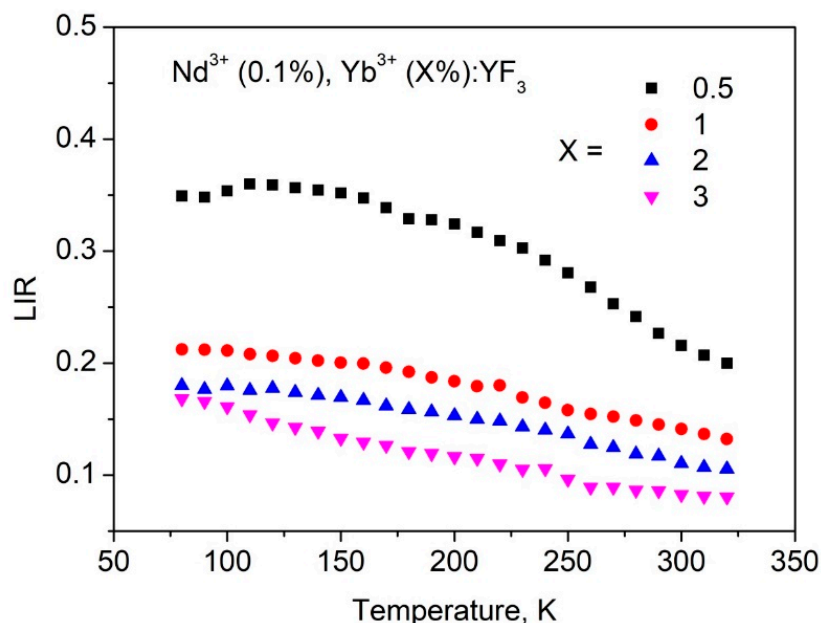
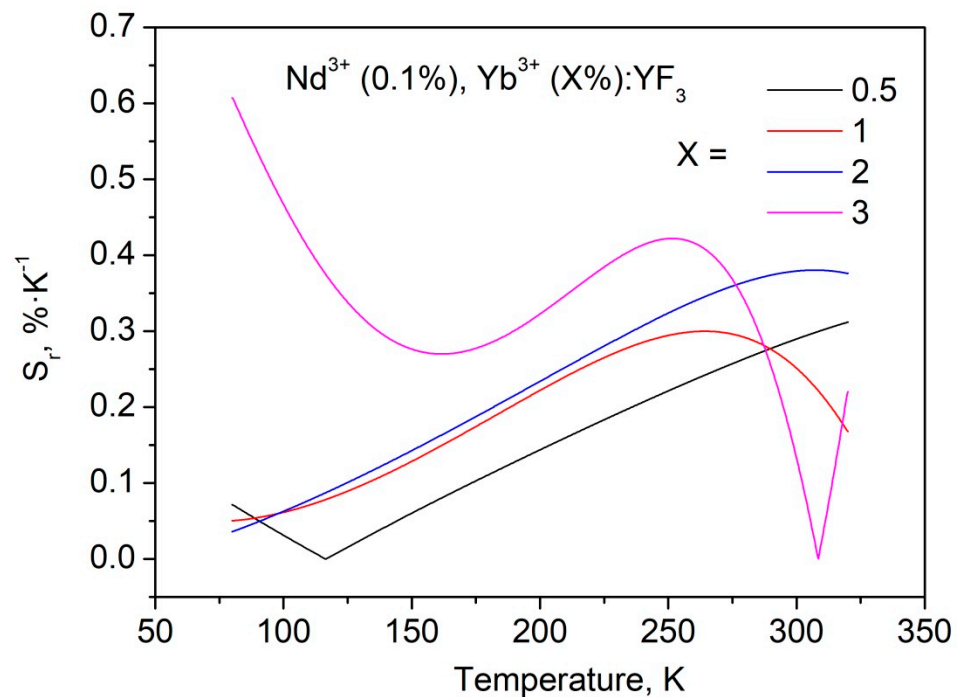


Figure 6. *LIR* as a function of temperature.

It can be seen, that all the luminescence intensity ratio (*LIR*) curves demonstrate decreasing behavior. It means, that  $\text{Yb}^{3+}$  intensity increases faster than  $\text{Nd}^{3+}$  one with the temperature increase. Such behavior of both intensities reflects the phonon-assisted nature of the energy transfer. Indeed, the efficiency of population of  $^2\text{F}_{5/2}$  ( $\text{Yb}^{3+}$ ) increases with the temperature increase as well as depopulation of  $^4\text{F}_{3/2}$  ( $\text{Nd}^{3+}$ ). The slight difference in *LIR* functions requires addition study, however, it can be suggested, that this difference related to back energy transfer from  $\text{Yb}^{3+}$  to  $\text{Nd}^{3+}$  that is different for different  $\text{Yb}^{3+}$  concentrations. Indeed, as we mentioned above, under  $\text{Nd}^{3+}$  excitation, the  $\text{Yb}^{3+}$  ions can obtain excitation energy. Further, there are at least three processes:  $\text{Yb}^{3+}$  emits the energy, it can transmit it back to  $\text{Nd}^{3+}$ , and  $\text{Yb}^{3+}$  can transmit it to  $\text{Yb}^{3+}$  (energy diffusion). These processes are competitive. In particular, the energy diffusion probability between  $\text{Yb}^{3+}$  ions increases with the increase of  $\text{Yb}^{3+}$  concentration. It also decreases the probability of back energy transfer to  $\text{Nd}^{3+}$ . For samples, having different concentrations of doping ions, the ratio between these probabilities is different that leads to difference in the shape of *LIR* curves. The estimation of contribution of the above-mentioned processes is one of the next steps of the present work. In order to calculate  $S_r$ , we used the equation:

$$S_r = \frac{1}{LIR} \left| \frac{d(LIR)}{dT} \right| \cdot 100\% \quad (1)$$

The  $S_r$  functions obtained from *LIR* curves are represented in Figure 7.



**Figure 7.**  $S_r$  as functions of temperature obtained from *LIR* curves for  $\text{Nd}^{3+}$  (0.1 mol.%),  $\text{Yb}^{3+}$  (X mol.%): $\text{YF}_3$  samples.

The obtained  $S_r$  values are quite competitive compared to our previous work [12]. As we mentioned above, for 0.5 and 1.0 mol.% single-doped  $\text{Nd}^{3+}$ : $\text{YF}_3$  the luminescence decay time of  $^4\text{F}_{3/2}$  ( $\text{Nd}^{3+}$ ) decreases with the temperature decrease in contrast to  $\text{Nd}^{3+}$  (0.1%): $\text{YF}_3$  sample. It was suggested, that depopulation of  $^4\text{F}_{3/2}$  level occurs via cross-relaxation. At lower temperatures the distance between  $\text{Nd}^{3+}$  ions decreases due to thermal expansion and the efficiency of quenching by cross-relaxation increases. In the case of 0.1 mol.%  $\text{Nd}^{3+}$  concentration, the distance between neighboring  $\text{Nd}^{3+}$  ions seems to be larger and the interaction between  $\text{Nd}^{3+}$  ions does not occur. In terms of luminescence thermometry, the higher concentration (0.5 and 1.0 mol.%) of  $\text{Nd}^{3+}$  for  $\text{Nd}^{3+}/\text{Yb}^{3+}$  ion pair seems to be more attractive. Indeed, the depopulation of  $^4\text{F}_{3/2}$  level happens via both cross-relaxation between  $\text{Nd}^{3+}$  ions and phonon-assisted energy transfer between  $\text{Nd}^{3+}$  and  $\text{Yb}^{3+}$ . It provides faster change of  $\text{Nd}^{3+}$  emission intensity or decay time with temperature compared to  $\text{Nd}^{3+}/\text{Yb}^{3+}$  doped samples, having 0.1 mol.% concentration of  $\text{Nd}^{3+}$ . This faster change of  $\text{Nd}^{3+}$  luminescence parameters can increase temperature sensitivity of  $\text{Nd}^{3+}$ ,  $\text{Yb}^{3+}$ : $\text{YF}_3$  samples. To verify this suggestion, we synthesized  $\text{Nd}^{3+}$  (0.5 mol.%),  $\text{Yb}^{3+}$  (0.5 and 1.0, mol.%): $\text{YF}_3$  nanoparticles via the same chemical method. However, in this system, further increase of  $\text{Yb}^{3+}$  content (higher than 1.0 mol.%) led to a significant increase of  $\text{Yb}^{3+}$  emission intensity and simultaneous decrease of  $\text{Nd}^{3+}$  one. This feature led to notable errors in *LIR* calculation. In turn,  $\text{Nd}^{3+}$  (1.0 mol.%): $\text{YF}_3$  showed notably low luminescence intensity due to concentration quenching (it also can be seen from luminescence decay time curves). Thus, we calculated  $S_r$  for two  $\text{Nd}^{3+}$  (0.5 mol.%),  $\text{Yb}^{3+}$  (0.5 and 1.0, mol.%): $\text{YF}_3$  samples (Figure 8).

It can be seen, that the obtained  $S_r$  values are higher compared to the  $S_r$  values calculated for  $\text{Nd}^{3+}$  (0.1 mol.%),  $\text{Yb}^{3+}$  (X mol.%): $\text{YF}_3$  samples at lower temperatures. Probably, the additional temperature-dependent depopulation of  $^4\text{F}_{3/2}$  level via cross-relaxation plays a crucial role in its temperature sensitivity in 80–150 K range. As it was mentioned above, the shape of the *LIR* curves is affected by the difficult competitive energy exchange processes between the doping ions. Since, the sensitivity curves are obtained from the *LIR* curves, their shapes differ between each other as well. Note, that the presence of the singular points is related to the fact, that we use absolute values (modulus) of the

sensitivity curves (Equation (1)). Hence in the area of the singular point without modulus, the  $S_r$  curve “goes” from positive part of XY plot to negative one or inversely. It can be seen, that the obtained  $S_r$  values are in the  $0.1\text{--}0.4\% \cdot \text{K}^{-1}$  in the physiological temperature range. These results are comparable to one of the main competitor  $\text{Nd}^{3+}$ ,  $\text{Yb}^{3+}:\text{LiLaP}_4\text{O}_{12}$  ( $0.1\text{--}0.3\% \cdot \text{K}^{-1}$ ) [15]. In the case of  $\text{Tm}^{3+}/\text{Yb}^{3+}$  down-conversion system operating in the biological window, the obtained  $S_r$  values also exceed the results obtained in [22]. It also should be noted, that the maximum  $S_r$  values are observed in the 80–150 K range. It can be concluded, that the synthesized phosphors are useful in cryogenic technique as well as in the space industry. The characterization of the present nanoparticles at lower temperatures is one of the next steps of the present study. Effective luminescence decay times  $\tau_{\text{eff}}$  ( ${}^4\text{F}_{3/2}\text{--}{}^4\text{I}_{9/2}$  transition, 866 nm emission) as functions of temperature for  $\text{Nd}^{3+}$  (0.5 mol.%),  $\text{Yb}^{3+}$  (X mol.%): $\text{YF}_3$  and  $\text{Nd}^{3+}$  (0.1 mol.%),  $\text{Yb}^{3+}$  (X mol.%): $\text{YF}_3$  are represented in Figure 9a,b, respectively.

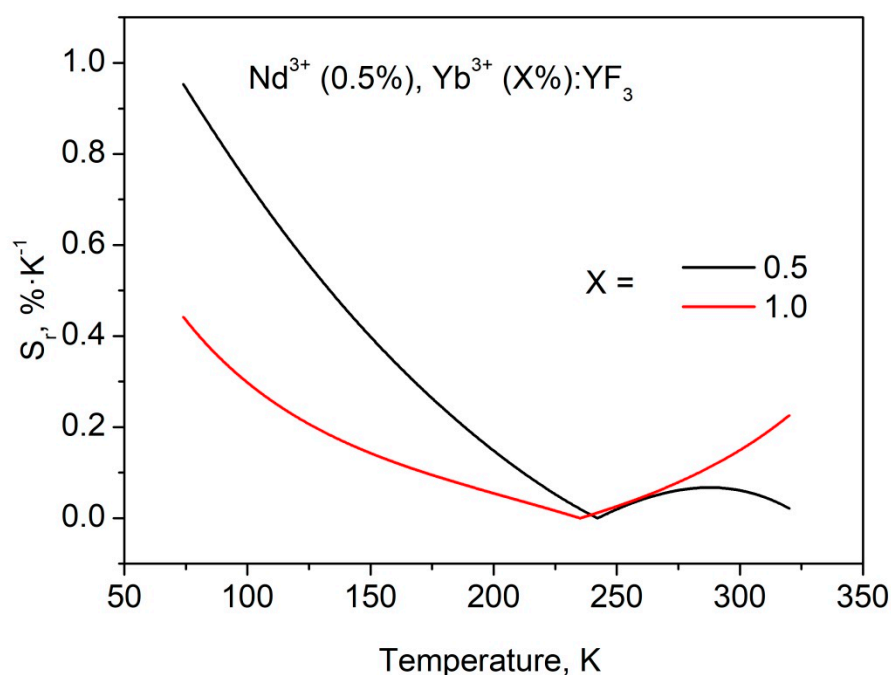


Figure 8.  $S_r$  a functions of temperature obtained from LIR curves for  $\text{Nd}^{3+}$  (0.1 mol.%),  $\text{Yb}^{3+}$  (X mol.%): $\text{YF}_3$  sample.

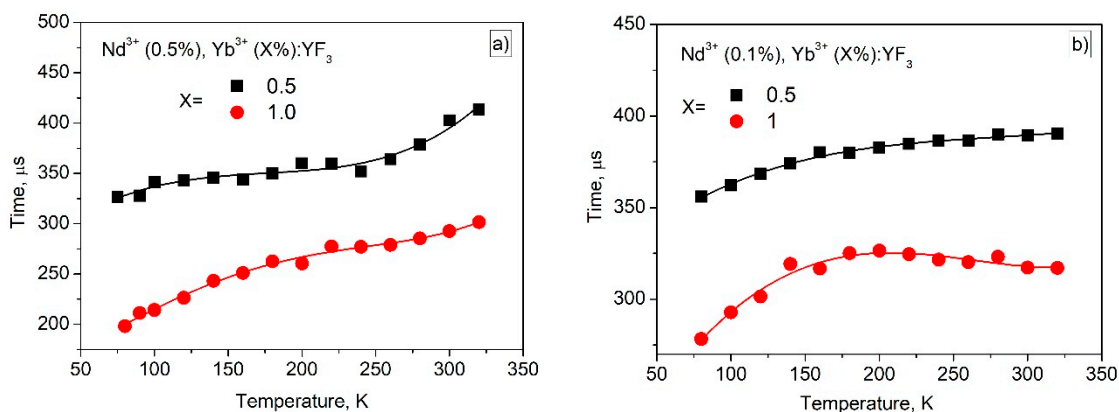


Figure 9. Effective luminescence decay times as functions of temperature for  $\text{Nd}^{3+}$  (0.5 mol.%),  $\text{Yb}^{3+}$  (X mol.%): $\text{YF}_3$  and  $\text{Nd}^{3+}$  (0.1 mol.%) (a),  $\text{Yb}^{3+}$  (X mol.%): $\text{YF}_3$  (b).

It can be seen, that the temperature dependence of  $\tau_{\text{eff}}$  of  $\text{Nd}^{3+}$  (0.5 mol.%),  $\text{Yb}^{3+}$  (X mol.%): $\text{YF}_3$  is more pronounced compared to  $\text{Nd}^{3+}$  (0.1 mol.%),  $\text{Yb}^{3+}$  (X mol.%): $\text{YF}_3$  sample. Indeed, for 0.5%  $\text{Nd}^{3+}$  sample  $\tau_{\text{eff}}$  changes in the  $\sim 100$   $\mu\text{s}$  time frame in opposite to 0.1%  $\text{Nd}^{3+}$  ( $\sim 50$   $\mu\text{s}$ ). It, also, can be related to the fact, that for 0.5 mol.%  $\text{Nd}^{3+}$  depopulation of  ${}^4\text{F}_{3/2}$  level occurs via cross-relaxation and phonon-assisted energy transfer in contrast to 0.1 mol.%  $\text{Nd}^{3+}$ . Finally, it can be concluded, that the  $\text{Nd}^{3+}$  (0.5 mol.%),  $\text{Yb}^{3+}$  (X mol.%): $\text{YF}_3$  samples are more effective for both ratiometric and lifetime temperature sensing especially in the 80–150 K range.

#### 4. Conclusions

This work was devoted to the study of thermometric performances of  $\text{Nd}^{3+}$  (0.1 or 0.5 mol.%),  $\text{Yb}^{3+}$  (X%): $\text{YF}_3$  nanoparticles. Firstly, the nanoparticles were characterized via well-known physical methods. Particularly, according to the TEM image, the nanoparticles demonstrate  $231 \pm 8$  nm average diameter. The obtained XRD patterns agree with both the simulation and the reference pattern from the Inorganic Crystal Diffraction Database of orthorhombic  $\text{YF}_3$  ( $P_{\text{nma}}$  space group (no. 074–0911)). Temperature sensitivity of spectral shape is related to the phonon-assisted nature of energy transfer (PAET) between  $\text{Nd}^{3+}$  and  $\text{Yb}^{3+}$ . However, in the case of single-doped  $\text{Nd}^{3+}$  (0.1 or 0.5 mol.%): $\text{YF}_3$  nanoparticles, luminescence decay time (LDT) of  ${}^4\text{F}_{3/2}$  level of  $\text{Nd}^{3+}$  in  $\text{Nd}^{3+}$  (0.5 mol.%): $\text{YF}_3$  decreases with the temperature decrease. In turn, luminescence decay time in  $\text{Nd}^{3+}$  (0.1 mol.%): $\text{YF}_3$  sample remains constant. It was proposed, that at 0.5 mol.% the cross-relaxation (CR) between  $\text{Nd}^{3+}$  ions takes place in contradistinction from 0.1 mol.%  $\text{Nd}^{3+}$  concentration. The decrease of LDT with temperature is explained by the decrease of distances between  $\text{Nd}^{3+}$  with temperature (thermal expansion phenomenon) that leads to the increase of cross-relaxation efficiency. It was suggested, that the presence of both CR and PAET processes in the studied ( $\text{Nd}^{3+}$  (0.5 mol.%),  $\text{Yb}^{3+}$  (X%): $\text{YF}_3$ ) nanoparticles provides higher temperature sensitivity compared to the systems having one temperature-dependent process ( $\text{Nd}^{3+}$  (0.1, 0.5 mol.%),  $\text{Yb}^{3+}$  (X%): $\text{YF}_3$ ). The experimental results confirmed this suggestion. The maximal relative temperature sensitivity was  $0.9\% \cdot \text{K}^{-1}$  at 80 K.

**Supplementary Materials:** The following supporting information can be downloaded at: <https://www.mdpi.com/article/10.3390/ma16010039/s1>, Figure S1: The luminescence spectra recorded at different values of power density of the laser irradiation; Figure S2: Room temperature luminescence spectrum of  $\text{Nd}^{3+}$  (0.1%),  $\text{Yb}^{3+}$  (3.0%): $\text{YF}_3$ .

**Author Contributions:** Conceptualization, M.P.; methodology, M.P., E.O., A.K. and M.C.; formal analysis, M.G.; investigation, M.P., E.O., A.K., M.C. and M.G.; resources, M.P. and M.G.; data curation, M.P. and E.O.; writing—original draft preparation, M.P.; project administration, M.P. and M.G.; funding acquisition, M.P. All authors have read and agreed to the published version of the manuscript.

**Funding:** This research was funded by the subsidy allocated to Kazan Federal University for the state assignment in the sphere of scientific activities (project number FZSM-2022-0021).

**Institutional Review Board Statement:** Not applicable.

**Informed Consent Statement:** Not applicable.

**Data Availability Statement:** Not applicable.

**Conflicts of Interest:** The authors declare no conflict of interest.

#### References

1. Jaque, D.; Vetrone, F. Luminescence nanothermometry. *Nanoscale* **2012**, *4*, 4301–4326. [[CrossRef](#)] [[PubMed](#)]
2. Brites, C.D.; Lima, P.P.; Silva, N.J.; Millán, A.; Amaral, V.S.; Palacio, F.; Carlos, L.D. Thermometry at the nanoscale. *Nanoscale* **2012**, *4*, 4799–4829. [[CrossRef](#)] [[PubMed](#)]
3. Wang, X.D.; Wolfbeis, O.S.; Meier, R.J. Luminescent probes and sensors for temperature. *Chem. Soc. Rev.* **2013**, *42*, 7834–7869. [[CrossRef](#)] [[PubMed](#)]
4. Hossain, M.K.; Ahmed, M.H.; Khan, M.I.; Miah, M.S.; Hossain, S. Recent Progress of Rare Earth Oxides for Sensor, Detector, and Electronic Device Applications: A Review. *ACS Appl. Electron. Mater.* **2021**, *3*, 4255–4283. [[CrossRef](#)]

5. Hossain, M.K.; Hossain, S.; Ahmed, M.H.; Khan, M.I.; Haque, N.; Raihan, G.A. A Review on Optical Applications, Prospects, and Challenges of Rare-Earth Oxides. *ACS Appl. Electron. Mater.* **2021**, *3*, 3715–3746. [[CrossRef](#)]
6. Piñol, R.; Brites, C.D.; Silva, N.J.; Carlos, L.D.; Millán, A. Nanoscale thermometry for hyperthermia applications. In *Nanomaterials for Magnetic and Optical Hyperthermia Applications*; Elsevier: Amsterdam, The Netherlands, 2019; pp. 139–172.
7. Bazhukova, I.N.; Pustovarov, V.A.; Myshkina, A.V.; Ulitko, M.V. Luminescent Nanomaterials Doped with Rare Earth Ions and Prospects for Their Biomedical Applications (A Review). *Opt. Spectrosc.* **2020**, *128*, 2050–2068. [[CrossRef](#)]
8. Fedorov, P.P.; Luginina, A.A.; Kuznetsov, S.V.; Osiko, V.V. Nanofluorides. *J. Fluor. Chem.* **2011**, *132*, 1012–1039. [[CrossRef](#)]
9. Pudovkin, M.S.; Zelenikhin, P.V.; Shtyreva, V.V.; Evtugyn, V.G.; Salnikov, V.V.; Nizamutdinov, A.S.; Semashko, V.V. Cellular uptake and cytotoxicity of unmodified Pr<sup>3+</sup>: LaF<sub>3</sub> nanoparticles. *J. Nanopart. Res.* **2019**, *21*, 184. [[CrossRef](#)]
10. Wang, X.; Li, Y. Rare-earth-compound nanowires, nanotubes, and fullerene-like nanoparticles: Synthesis, characterization, and properties. *Chem.-A Eur. J.* **2003**, *9*, 5627–5635. [[CrossRef](#)]
11. Ximendes, E.C.; Rocha, U.; Kumar, K.U.; Jacinto, C.; Jaque, D. LaF<sub>3</sub> core/shell nanoparticles for subcutaneous heating and thermal sensing in the second biological-window. *Appl. Phys. Lett.* **2016**, *108*, 253103. [[CrossRef](#)]
12. Pudovkin, M.S.; Ginkel, A.K.; Lukinova, E.V. Temperature sensitivity of Nd<sup>3+</sup>, Yb<sup>3+</sup>: YF<sub>3</sub> ratiometric luminescent thermometers at different Yb<sup>3+</sup> concentration. *Opt. Mater.* **2021**, *119*, 111328. [[CrossRef](#)]
13. Aarts, L.; Ende, B.V.D.; Reid, M.F.; Meijerink, A. Downconversion for solar cells in YF<sub>3</sub>: Pr<sup>3+</sup>, Yb<sup>3+</sup>. *Spectrosc. Lett.* **2010**, *43*, 373–381. [[CrossRef](#)]
14. Marciniak, L.; Bednarkiewicz, A.; Trejgis, K.; Maciejewska, K.; Elzbiaciak, K.; Ledwa, K. Enhancing the sensitivity of a Nd<sup>3+</sup>, Yb<sup>3+</sup>: YVO<sub>4</sub> nanocrystalline luminescent thermometer by host sensitization. *Phys. Chem. Chem. Phys.* **2019**, *21*, 10532–10539. [[CrossRef](#)] [[PubMed](#)]
15. Bednarkiewicz, A.; Stefanski, M.; Tomala, R.; Hreniak, D.; Strek, W. Near infrared absorbing near infrared emitting highly-sensitive luminescent nanothermometer based on Nd<sup>3+</sup> to Yb<sup>3+</sup> energy transfer. *Phys. Chem. Chem. Phys.* **2015**, *17*, 24315–24321.
16. Pudovkin, M.S.; Ginkel, A.K.; Morozov, O.A.; Kiiamov, A.G.; Kuznetsov, M.D. Highly-sensitive lifetime optical thermometers based on Nd<sup>3+</sup>, Yb<sup>3+</sup>: YF<sub>3</sub> phosphors. *J. Lumin.* **2022**, *249*, 119037. [[CrossRef](#)]
17. Kaczmarek, A.M.; Kaczmarek, M.K.; Van Deun, R. Er<sup>3+</sup>-to-Yb<sup>3+</sup> and Pr<sup>3+</sup>-to-Yb<sup>3+</sup> energy transfer for highly efficient near-infrared cryogenic optical temperature sensing. *Nanoscale* **2019**, *11*, 833–837. [[CrossRef](#)]
18. Maciejewska, K.; Bednarkiewicz, A.; Marciniak, L. NIR luminescence lifetime nanothermometry based on phonon assisted Yb<sup>3+</sup>–Nd<sup>3+</sup> energy transfer. *Nanoscale Adv.* **2021**, *3*, 4918–4925. [[CrossRef](#)]
19. Rocha, U.; Upendra Kumar, K.; Jacinto, C.; Ramiro, J.; Caamano, A.J.; Garcia Sole, J.; Jaque, D. Nd<sup>3+</sup> doped LaF<sub>3</sub> nanoparticles as self-monitored photo-thermal agents. *Appl. Phys. Lett.* **2014**, *104*, 053703. [[CrossRef](#)]
20. Wang, X.; Xu, T.; Cai, P.; Vu, T.; Seo, H.J. Controlled synthesis, multicolor luminescence, and optical thermometer of bifunctional NaYbF<sub>4</sub>: Nd<sup>3+</sup>@NaYF<sub>4</sub>: Yb<sup>3+</sup> active-core/active-shell colloidal nanoparticles. *J. Alloys Compound.* **2017**, *691*, 530–536. [[CrossRef](#)]
21. Vanetsev, A.; Kaldvee, K.; Puust, L.; Keevend, K.; Nefedova, A.; Fedorenko, S.; Orlovskii, Y. Relation of Crystallinity and Fluorescent Properties of LaF<sub>3</sub>: Nd<sup>3+</sup> Nanoparticles Synthesized with Different Water-Based Techniques. *Chem. Select* **2017**, *2*, 4874–4881. [[CrossRef](#)]
22. Khadiev, A.R.; Korableva, S.L.; Ginkel, A.K.; Morozov, O.A.; Nizamutdinov, A.S.; Semashko, V.V.; Pudovkin, M.S. Down-conversion based Tm<sup>3+</sup>: LiY<sub>1</sub>-XYbXF<sub>4</sub> temperature sensors. *Opt. Mater.* **2022**, *134*, 113118. [[CrossRef](#)]

**Disclaimer/Publisher’s Note:** The statements, opinions and data contained in all publications are solely those of the individual author(s) and contributor(s) and not of MDPI and/or the editor(s). MDPI and/or the editor(s) disclaim responsibility for any injury to people or property resulting from any ideas, methods, instructions or products referred to in the content.